Check for updates

ADVANCED ENERGY MATERIALS
www.advenergymat.de

A Novel Plastic-Crystal Electrolyte with Fast Ion-Transport Channels for Solid Zinc-Ion Batteries

*Zhiming Zhao, Binbin Nian, Yongjiu Lei, Yizhou Wang, Lin Shi, Jian Yin, Omar F. Mohammed, and Husam N. Alshareef**

Miniaturized solid zinc-ion batteries that are safe, environmentally friendly, and low-cost are ideal candidates for powering emerging microelectronics. However, sluggish Zn^{2+} mobility in solid phases hampers the viability of solid Zn^{2+} electrolytes and hence their practicability. Here, nanoscale Zn^{2+} channels are successfully engineered in a plastic-crystal electrolyte, thus activating fast Zn^{2+} solid-state transport. The ion-dipole interaction exerted by water molecules orients amphiphilic anions in bilayers, further forming a layered architecture backed by long-range van der Waals attractive forces. In the interlayer, the heteroleptic coordination contributed by the water molecule and anion frees the Zn^{2+} from anionic traps, leading to a high Zn^{2+} conductivity of 2.2×10^{-3} S cm^{-1}. This elaborately tailored texture confers a combination of robust mechanical characteristics and outstanding electrochemical performance upon the resultant electrolyte. The applicability is demonstrated by the high Zn^{2+} platting/stripping efficiency (99.6%), durable longevity of symmetric Zn-Zn and Zn-MnO_2 cells, as well as the engineering of versatile micro batteries (MBs). This work provides new perspectives for developing super multivalent ion conductors through the innovative design of ion-conducting nanochannels.

1. Introduction

Zinc (Zn)-ion batteries (ZIBs) have received a plethora of spotlights in the latest decade, most of which indulge in aqueous electrolyte systems that utilize water as the solvent.[1] However, a harsh fact is that the relatively low energy density (below 40 Wh kg^{-1}) derived from a high redox potential of the Zn anode (−0.76 V) makes it difficult for ZIBs to compete with lithium-ion batteries in routine applications, such as portable devices and electric vehicles.[2] The poor reversibility of Zn metal in aqueous electrolytes induced by inherent thermodynamic instability and dendrite issue further devalues their applicability.[2a,3] In this regard, ZIBs are indeed more suitable for scenarios that do not entail high gravimetric energy density, encompassing stationary energy storage systems and micro devices such as wearable devices, audiphones, and so forth. The applications of ZIBs in miniaturized devices rely on the strength of solid electrolytes that demonstrate attributes of solidity, flexibility, mechanical durability, and importantly, practical ionic conductivity.[4] However, the high charge capacity of divalent Zn^{2+} tends to induce strong interactions with the surrounding matrix and corresponding mass diffusion barriers in solid phases, placing a formidable challenge on eligible ion transport. In this vein, seminal classes of strategies were proposed, highlighting that Zn^{2+} transport would be facilitated by mastering host morphological structure,[5] modulating the Zn^{2+} coordination environment,[6] as well as constraining counter anions.[7] Despite these contributions, unfortunately, a practical conductivity in the magnitude of 10^{-3} S cm^{-1} is still unattainable.

Recently, the nano-regime has offered "new degrees of freedom" for fostering ion transport in the solid phase and solid state electrochemistry.[8] It turned out that superb ion conduction can be promised by utilizing mesoporous insulator phases with pore sizes of certain nanometers.[9] High storage and prompt exchange of energy and information on an instant timescale are permitted as the channels involved in the regime are at nano levels. This nano-size effect was highlighted as a "quantum-confined superfluid" concept in fluid mechanics.[10] A representative of this concept is the integration of biological functions essentially connected with nano-structuring, allowing ultrafast ionic transport of 10^7 ions across per channel in 1 s to realize prompt information exchange.[11] Briefly speaking, ion transport in nanochannels by a regular array is pronouncedly faster than in a chaotic way due to trivial and nontrivial size

Z. Zhao, Y. Lei, Y. Wang, L. Shi, J. Yin, H. N. Alshareef
Materials Science and Engineering
Physical Science and Engineering Division
King Abdullah University of Science and Technology (KAUST)
Thuwal 23955–6900, Kingdom of Saudi Arabia
E-mail: husam.alshareef@kaust.edu.sa
B. Nian
School of Pharmaceutical Sciences
Nanjing Technology University
Nanjing, Jiangsu Province 210009, P. R. China
O. F. Mohammed
Advanced Membranes and Porous Materials Center
KAUST Catalysis Center
Physical Science and Engineering Division
King Abdullah University of Science and Technology
Thuwal 23955-6900, Kingdom of Saudi Arabia

The ORCID identification number(s) for the author(s) of this article can be found under https://doi.org/10.1002/aenm.202300063

DOI: 10.1002/aenm.202300063

 © 2023 Wiley-VCH GmbH

effects.[8] In doing so, it becomes possible to provoke the multivalent Zn^{2+} conduction in solid phases on the strength of constructing nano transport channels.

Here, we describe a plastic-crystal Zn^{2+} electrolyte with nano-conducting pathways created by the self-assembly of amphiphilic anions, accessing an appreciable ionic conductivity of 3×10^{-3} S cm^{-1}. The ion-dipole interaction between the water molecule and the bis(2-ethylhexyl) sulfosuccinate (Aerosol-OT, AOT) anions confines the AOT in a finite layer, forming a layered structure and warranting a high Zn^{2+} transference number of 0.73. Concomitantly, the water molecules in the interlayers solvate Zn^{2+} by heteroleptic coordination, which frees Zn^{2+} from anionic traps and pronouncedly minimizes its migration barriers in the nanochannels. Notably, the water molecules in the interlayers are mainly in ligand form, suppressing their incompatibility with Zn anodes. This customized electrolyte endows Zn-Cu, Zn-Zn, and Zn-MnO_2 batteries with significant rechargeability. The demonstration of integrative Zn-MnO_2 micro batteries with high reversibility signifies the versatility and practicability of our electrolytes. This study underscores the importance of architecting ion-transport channels in improving cationic mobility in a solid matrix.

2. Results and Discussions

Few inorganic solid-state electrolytes (SSEs) with good Zn^{2+} conductivity were reported since Zn^{2+} is hardly mobile in crystals, albeit with some systems operating at extremely high temperatures.[12] Also, it is not easy to construct conduction channels for Zn^{2+} in conventional polymer media (such as polyethylene oxide (PEO), polyethylene glycol (PEG), and polyvinylidene fluoride (PVDF)). Cross-linking of the polar counter sites of the polymer matrix often occurs on the center of the multivalent Zn^{2+} carrying a high charge density, inducing shackle-like intrachain chelation or local networks.[6a] Thus, in an attempt to engineer fast conduction channels for Zn^{2+} in a solid phase, a radical top-down strategy is necessitated starting from the original molecule-level design. It is known that the system comprising polar, apolar, and amphiphilic molecules can form self-assembled configurations with ordered microstructures in the appropriate concentration range. AOT, a classical amphiphilic anion with abundant hydrophilic sites on the head and two distant hydrophobic tails (Figure S1, Supporting Information), is widely used in a range of applications from templates for semiconductors,[13] to models for biological membranes,[14] and to restricted nano parclose for chemistry.[15] Nevertheless, the possible application of AOT on the morphological architecture of solid electrolytes has yet to be explored.

To resort to the self-assembly ability of AOT anions and realize the construction of Zn^{2+} conduction capillaries in the solid phase, we synthesized $Zn(AOT)_2$ via a facile ion exchange reaction (See Methods in the Supporting Information). The pure $Zn(AOT)_2$ salt shows as white solids and exhibits similar XRD patterns with NaAOT (**Figure 1**a, FigureS2, Supporting Information). However, once 20 wt.% water is consolidated with $Zn(AOT)_2$, the complex turns to a translucent waxy state with good ductility and is named as ZPE (abbreviation of **Z**n^{2+} **p**lastic-crystal **e**lectrolytes) (Figure 1b). As ZPE was coated on a polyamide separator, a semitransparent electrolyte membrane can be obtained with a thickness of 120 μm (Figure 1c-e), which was adopted as the self-supported electrolyte in this work. As presented in the optical images (Figure 1d), the electrolyte membrane shows good flexibility, which can be freely bent and folded.

In a typical solid battery with a sandwich structure, relative displacement of the components accompanied by interfacial cracks often occur due to the rigid mechanical coupling between the electrode and electrolyte. To accommodate these interfacial issues, ideally, the electrolyte needs to tightly comply with the electrode by synchronously elongating/shrinking in a continuously dynamic state (Figure S3, Supporting Information). To this end, multiple mechanical properties including reversible stretchability and appropriate viscoelasticity are required for the electrolyte. To detect these mechanical properties, a tensile test was first demonstrated. As shown in Figure 1f, the electrolyte membrane can be stretched by 200% deformation and nearly restored to its original state once relaxing, verifying its reversible stretchability. A rheology study was then carried out to explore the elastic and viscous properties, which can be characterized by storage modulus (G') and loss modulus (G''), respectively. The modulus evolution accompanying frequency sweeping is illustrated in Figure 1g. In the lower frequency range (<1 rad s^{-1}), a larger G'' than G' can be gauged, suggesting that the viscosity is the dominant property in a terminal region that mainly responds to weak strain. However, once the angular frequency is above 1 rad s^{-1}, a greatly increased G' was measured, which significantly exceeds G'', suggesting a rubbery region was reached.[16] The demise of G'' to G' implies that ZPE will become stiff once it encounters a large force, which is a crucial manner to resist external deformation for solid batteries.[17] Additionally, the complex viscosity changes linearly with the frequency as in the logarithmic form, suggesting the non-Newtonian characteristic and solid nature of ZPE (Figure 1h).[18] In short, these mechanical flexibility and durability are anticipated to bestow solid batteries with compatible interfaces and robustness by alleviating structural dislocations.

Having shown the mechanical robustness, our attention then turned to disclose the micro configuration of ZPE. Our first attempt is to determine the water existence form in ZPE to set our work apart from gel electrolytes where free water extensively exists. The O–H stretching vibration mode was thus studied by FTIR, considering its sensitivity to the chemical atmosphere. As apparent from **Figure 2**a, a much sharper vibration band situated at 3414 cm^{-1} is observed in ZPE, displaying a substantial blue shift relative to pure water (3259 cm^{-1}), which is characteristic of crystalline hydrates and has rarely been observed in routine aqueous solutions.[19] To reinforce this observation, differential scanning calorimetry (DSC) was performed (Figure 2b). We found that the water in ZPE starts to evaporate at a high temperature of 106 °C, affirming that the ligand water is dominant in ZPE. The same conclusion could be drawn from a volatilization test (Figure S4, Supporting Information). ZPE was set in an open evaporation pan at room temperature and relative humidity of ≈50%. After one week, the water weight shows an imperceptible loss (1.52%). This water-retention property is helpful to the battery with an open system to obviate the drying up of electrolytes, favored by the absence of free water in ZPE.

The chemical motif of AOT was then investigated, considering that its amphiphilicity will dictate the ZPE architecture. As the hydrophilic and hydrophobic ends, the sulfonate and methyl

© 2023 Wiley-VCH GmbH

16146840, 2023, 21, Downloaded from https://advanced.onlinelibrary.wiley.com/doi/10.1002/aenm.202300063 by - Jilin University , Wiley Online Library on [27/03/2025]. See the Terms and Conditions (https://onlinelibrary.wiley.com/terms-and-conditions) on Wiley Online Library for rules of use; OA articles are governed by the applicable Creative Commons License

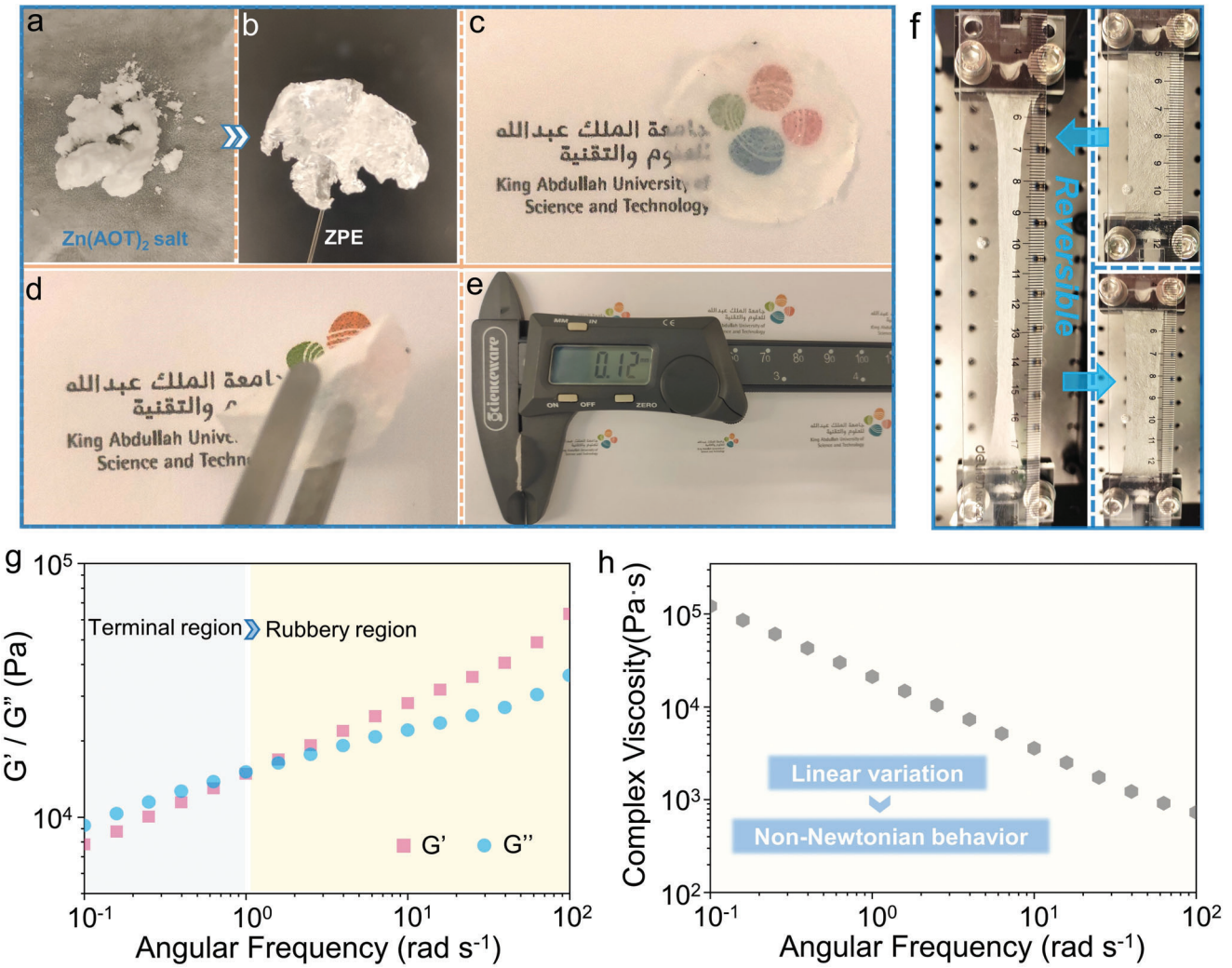

Figure 1. Digital photographs of a) the synthesized $Zn(AOT)_2$ salt, (b) the Zn^{2+} plastic-crystal electrolytes (ZPE), c-d) the flexible electrolyte membrane prepared by coating ZPE on polyamide 6 nonwovens, and e) the thickness measurement of the electrolyte membrane. f) The tensile test for the electrolyte membrane. g) Rheological study of ZPE (G′ and G″ represent storage modulus and loss modulus, respectively). h) Complex viscosities of ZPE versus angular frequency.

groups are studied respectively by FTIR (Figure 2c). Compared to pure $Zn(AOT)_2$, the symmetric stretching mode of sulfonate (ν_s (SO_3)) demonstrates a shift to a lower wavenumber in ZPE, reflecting a reduction in the strength of the sulfonate-Zn^{2+} interaction due to the hydration effect. This weaker interaction was further corroborated by the essential decrease in the FWHM (full-width-at-half-maximum), which derives from a faster vibrational relaxation rate tied to the disassociation between AOT and Zn^{2+}, accompanied by the substitution of interaction between the water molecule and AOT.[20] Considering the significant dipole moment ($\mu = 1.86$ D) of the water molecule, the attractive force between the water molecule and AOT can be attributable to the anion-dipole interaction.[21] By comparison, both the symmetrical stretching vibration (ν_s (CH_3)) and antisymmetric stretching vibration (ν_{as} (CH_3)) of the methyl group in ZPE show no change relative to pure $Zn(AOT)_2$, inferring that AOT anions are oriented towards water molecules by the hydration of sulfonate ends, which renders the feasibility of assembling ordered patterns. To scrutinize this possibly well-organized framework, small angle X-ray diffraction (SAXD) was performed. As shown in Figure 2d, there is only one peak in the vicinity of 3.66° for pure $Zn(AOT)_2$ salt, which is invalid to determine the crystalline structure. However, once 20 wt.% water is incorporated into $Zn(AOT)_2$, two intense peaks located at 3.24° and 6.51° arise, corresponding to a d value of 2.72 and 1.36 nm, respectively. Encouragingly, we notice that these d values exhibit two-fold relations, leading us to speculate that these two diffraction signals are likely attributed to the (0 0 2) and (0 0 4) planes of a layered matrix, respectively.

To offer a theoretical juxtaposition to the above experimental results, we applied molecular dynamics (MD) simulations to further examine the microscopic fabric of ZPE. **Figure 3**a displays a typical interlayer environment obtained from the equilibrium trajectory. As anticipated, the water molecules play an anchor role in drawing the hydrophilic sulfonate head of AOT toward them, while they are forbidden from approaching the hydrophobic

© 2023 Wiley-VCH GmbH

16146840, 2023, 21, Downloaded from https://advanced.onlinelibrary.wiley.com/doi/10.1002/aenm.202300063 by - Jilin University , Wiley Online Library on [27/03/2025]. See the Terms and Conditions (https://onlinelibrary.wiley.com/terms-and-conditions) on Wiley Online Library for rules of use; OA articles are governed by the applicable Creative Commons License

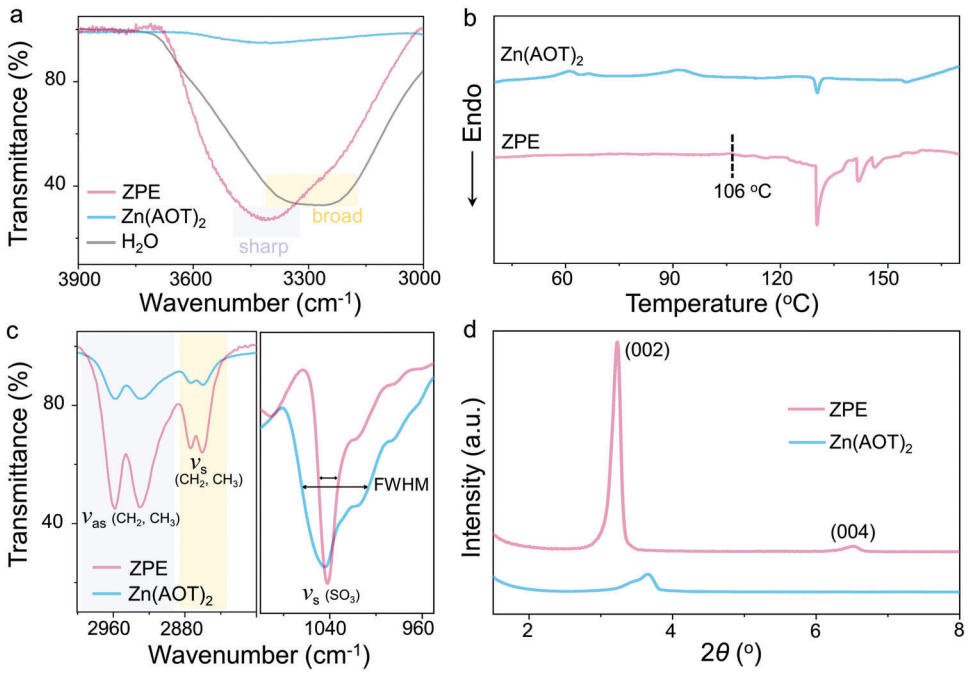

Figure 2. a) FTIR spectra of different samples in the range of 3000–3900 cm^{-1}. b) DSC-TA test at a healing rate of 5 °C min^{-1}. c) FTIR spectra corresponding to methyl stretching mode (left) and symmetric sulfonate stretching mode (right). d) Small angle X-ray diffraction (SAXD) of pure $Zn(AOT)_2$ and ZPE (The abscissa axis is shown in 2θ form).

methyl tails, leading to the oriented AOT arrays. The quantitative analysis of the radial distribution functions (RDFs) indicates that they interact with the sulfonate group within a distance of 1.8 Å (Figure 3b), mediated by an ion-dipole function (Figure S5-6, Table S1, Supporting Information). SAXD simulations were further conducted to ascertain the regular spread of AOT anions (Figure 3c). As expected, the diffraction vectors exhibit a geometric progression of 2.82, 5.64, and 11.28 nm^{-1}, apparently corresponding to (0 0 2), (0 0 4), and (0 0 6) planes of a typical layered structure. Between every two layers, abundant reticular ion channels are thus formed. On the other hand, the water molecules contribute themselves to the Zn^{2+} solvation shell by cooperating with AOT. According to RDF results, the solvation shell of Zn^{2+} is approximately composed of 4 water molecules and 1 AOT anion, accompanied by a similar function distance of 1.9 Å (Figure 3d). This heteroleptic coordination is anticipated to significantly activate Zn^{2+} transport where the ligand water acts as a lubricant (Figure S7, Supporting Information). To prove this hypothesis, the diffusion coefficient was determined by calculating the mean-squared displacements (MSDs) (Figure 3e). We notice that the long-term Stokes–Einstein diffusion coefficient of Zn^{2+} in ZPE is two orders of magnitude greater than in the system free of water, validating that the solid electrostatic coupling between Zn^{2+} and AOT is alleviated thanks to the presence of water in Zn^{2+} solvation shell. Based on the Zn^{2+} solvation model obtained from MD simulations, density functional theory (DFT) calculations were further performed to decipher the binding energy among diverse ligands. Our results identify that the Zn^{2+} de-solvation energy from the solvate complex in ZPE is less than half of that in $Zn(AOT)_2$ (inset of Figure 3e, Figure S8, Tables S2–S3, Supporting Information). The decreased de-solvation energy manifests that fewer driving forces are required for Zn^{2+} transfer between continuous complex sites in ZPE and ensures lower energy hysteresis of Faradic reactions, conducive to fast and reversible electrochemical kinetics. These theoretical analyses agree well with the experimental results, justifying the force field adopted in the MD simulations.

On the basis of the combined experimental and computational results, it becomes possible to clarify ZPE configuration (Figure 3f). In pure $Zn(AOT)_2$, encapsulated ionic bonds clamp Zn^{2+} in its fixed lattice site where only puny Brownian motion exists and appreciable ion conduction never occurs. However, the intervention of water provokes the destiny alternation of $Zn(AOT)_2$, transferring it to a fast ionic conductor (conductivity: 3×10^{-3} S cm^{-1}, Figure S9, Supporting Information). In this process, the water molecules play two key roles: 1) they lure the hydrophilic sulfonate in AOT close to them whereas repelling the hydrophobic methyl away from them. The long-range van der Waals attractive forces further help the architecture of a layered fabric, where two reversed AOT sublayers compose one layer wall while Zn^{2+} and the water molecules parasitize in the nanochannels between every two walls; 2) the water molecules in the nanochannels participate in Zn^{2+} solvation shell, which partially substitute for the AOT anions that strongly shackle Zn^{2+}, concurrently shielding the negative charge attraction from AOT walls. Backed by these crucial short-range interactions and long-range forces, the construction of nano transport channels and corresponding fast Zn^{2+} conduction is thus realized. Noteworthy is that the AOT anions are programmed into a crystalline lattice, but a fluctuational degree of freedom is retained in the internal channels of ZPE. Thereby, this new type of electrolyte actually belongs to generalized plastic crystals.[22]

© 2023 Wiley-VCH GmbH

16146840, 2023, 21, Downloaded from https://advanced.onlinelibrary.wiley.com/doi/10.1002/aenm.202300063 by - Jilin University , Wiley Online Library on [27/03/2025]. See the Terms and Conditions (https://onlinelibrary.wiley.com/terms-and-conditions) on Wiley Online Library for rules of use; OA articles are governed by the applicable Creative Commons License

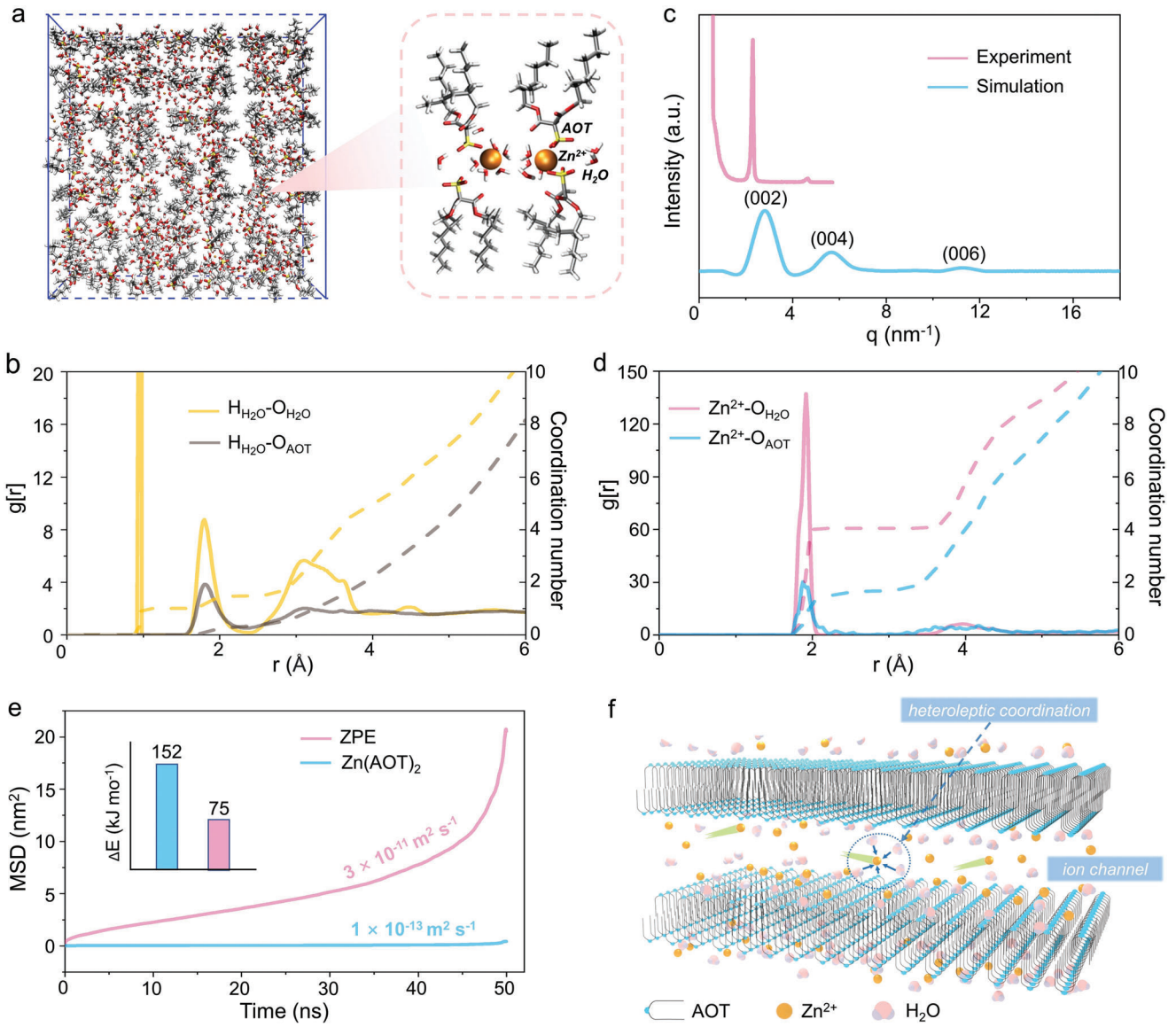

Figure 3. a) Snapshot from the equilibrium trajectory of the molecular dynamics simulation. b) The radial distribution function (RDF, g[r]) curve and coordination number for H_{H2O}-O_{H2O} and H_{H2O}-O_{AOT} (SO_3^-). c) SAXD patterns obtained by experiment and simulation (The abscissa axis is shown in diffraction vector *q* form). d) Radial distribution function (RDF, g[r], solid lines) curve and coordination number (dashed lines) for Zn^{2+}-O_{H2O} and Zn^{2+}-O_{AOT} (SO_3^-). e) Mean-squared displacement (MSD) of Zn^{2+} in ZPE and $Zn(AOT)_2$ from the position at time 0 (Inset: the de-solvation energy of Zn^{2+} in ZPE (red color) and $Zn(AOT)_2$ (blue color)). f) Schematic representation of the layered structure of ZPE.

So far, we have managed to architect Zn^{2+} conduction nanochannels by utilizing the self-assembly of amphiphilic AOT anions. We then study how this well-designed texture affects the electrochemical properties from multiple perspectives. The anodic stability (related to the OER) and cathodic stability (related to HER) were first analyzed (**Figure 4**a). The results show that no apparent decomposition current is detected before the bulk reduction of Zn^{2+} on the cathodic side. On the anodic side, the oxidation voltage of ZPE even exceeds 2.8 V (vs Zn/Zn^{2+}, 5 V Li/Li^+). These results again prove that the water molecules in ZPE are coordinated and form stable solvates, bestowing ZPE with a wide electrochemical window. Additionally, the immobilization of AOT anions in the layered walls is expected to facilitate the transport of counter ions; the Zn^{2+} transference number was thus identified (Figure 4b). Based on the Bruce-Vincent methodology, a high Zn^{2+} transference number of 0.73 is accessed, which suggests that a large amount of available Zn^{2+} flux and a fortified mass transfer rate between ZPE and metallic Zn electrode would be raised in the charge/discharge process, hence warranting the uniformity of Zn deposition and dissolution behavior (as will be discussed later). Correspondingly, a high Zn^{2+} conductivity of 2.2 × 10^{-3} S cm^{-1} is thus obtained. The Coulombic efficiency (CE) in Zn–Cu cells is furthermore evaluated (Figure 4c). At a current density of 1 mA cm^{-2}, a high average CE of 99.62 (after the initial 20 cycles) together with ultra-stable voltage curves responding to Zn^{2+} deposition/dissolution are acquired (Figure

© 2023 Wiley-VCH GmbH

16146840, 2023, 21, Downloaded from https://advanced.onlinelibrary.wiley.com/doi/10.1002/aenm.202300063 by - Jilin University , Wiley Online Library on [27/03/2025]. See the Terms and Conditions (https://onlinelibrary.wiley.com/terms-and-conditions) on Wiley Online Library for rules of use; OA articles are governed by the applicable Creative Commons License

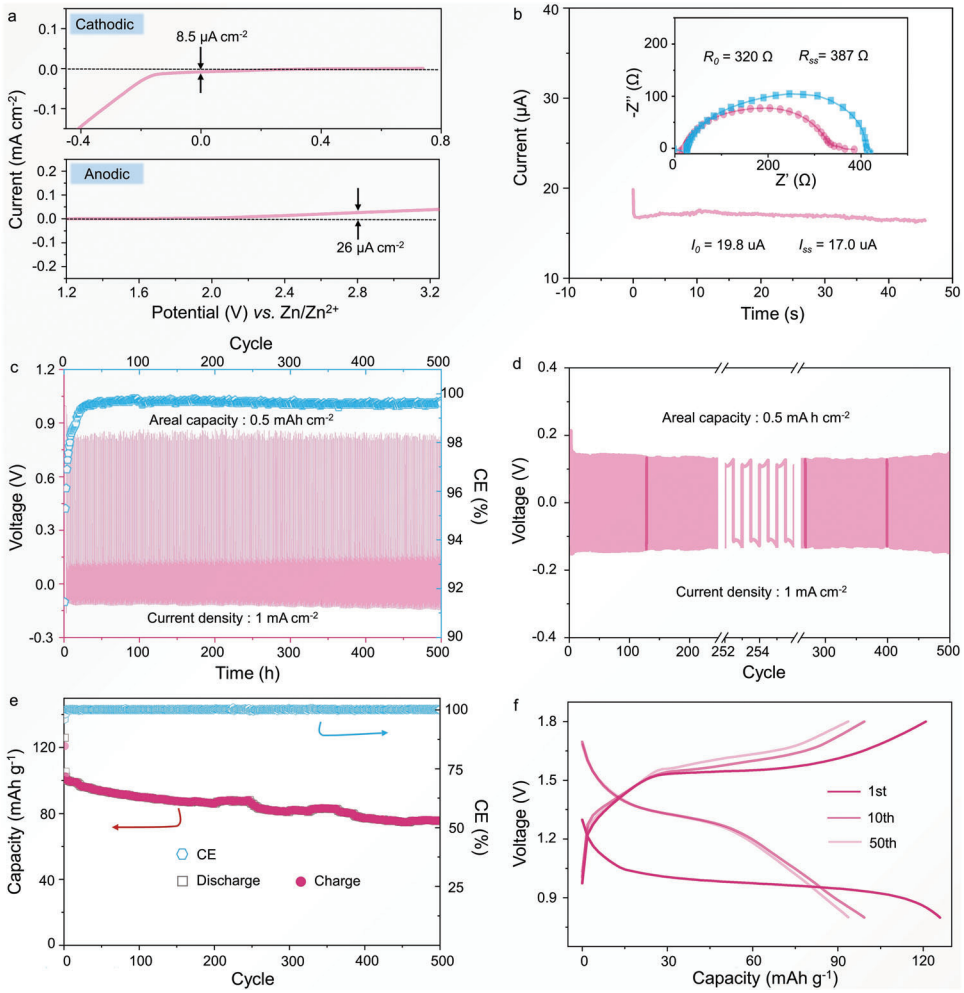

Figure 4. a) Linear sweep voltammograms (LSV) detected at a scanning rate of 1 mV s^{-1} in a three-electrode system (RE: Ag/AgCl; CE: carbon cloth; WE: Titanium (Ti) plate). b) Test of Zn^{2+} transference of ZPE. Direct current (DC) polarization curve of the symmetrical Zn cells at a constant voltage of 0.005 V (Inset shows the impedance plot before and after DC polarization of symmetrical cell). c) CE of Zn^{2+} plating/stripping on Cu substrate with an areal capacity of 0.5 mA h cm^{-2} (current density: 1 mA cm^{-2}). d) Cycling performance of a symmetric Zn cell with ZPE (1 mA cm^{-2}, 0.5 mA h cm^{-2}). e) Cycling performance of Zn-MnO_2 battery at a current density of 200 mA g^{-1}. f) Charge-discharge curves of Zn-MnO_2 battery at different cycles corresponding to Figure 4e.

S10, Supporting Information), suggesting the cells incorporating ZPE should be long-lasting and enable high energy efficiency. By using a symmetrical Zn cell under galvanostatic conditions to create the continuous transition between Zn^0 and Zn^{2+}, we could discriminate and foretell the anode longevity separately from the cathodes as applied in full batteries. As illustrated in Figure 4d, the cell exhibits stable polarization voltages for over 500 h at a current density of 1 mA cm^{-2} (0.5 mAh cm^{-2}). The XRD pattern of the cycled Zn electrode disassembled from the deposition side manifests that the deposition layer is predominantly zerovalent Zn (Figure S11, Supporting Information). Notably, the Zn surface retains a smooth morphology with no apparent dendrite observed (Figure S12, Supporting Information). We further found that ZPE is rate-tolerant which can support a high current density of 3 mA cm^{-2} with an areal capacity of 1.5 mAh cm^{-2} (Figure S13, Supporting Information). This is remarkable, especially considering the formidable mass diffusion barrier and sluggish kinetics of divalent Zn^{2+} in solid phases.[2b]

After affirming the integrity of the basic electrochemical parameters of ZPE, full prototype Zn-MnO_2 batteries were assembled to check the practical applicability. We used interlaminated δ-MnO_2 here mainly because it owns an ample interlayer space (≈7 Å), which may facilitate Zn^{2+} intercalation from solid phases.[23] As depicted in Figure 4e, the Zn-MnO_2 cell displays stable cycling for over 500 cycles with a high CE approaching 100% under galvanostatic conditions. No perceptible changes in the voltage hysteresis can be observed during cycling (Figure 4f), benefiting from the suppressed side reactions (e.g., Mn dissolution, Zn passivation) and good chemical compatibility of ZPE toward active materials. It should be noted that the intricate energy storage mechanism of δ-MnO_2 is not easy to uncover, leading to a debatable but intriguing topic in the community recently, which is not the core concern of this work.[24]

Microelectronic devices have been widely commercialized, which raises huge demands for easy-to-fabricate miniaturized energy carriers. In view of its good mechanical properties and

© 2023 Wiley-VCH GmbH

16146840, 2023, 21, Downloaded from https://advanced.onlinelibrary.wiley.com/doi/10.1002/aenm.202300063 by - Jilin University , Wiley Online Library on [27/03/2025]. See the Terms and Conditions (https://onlinelibrary.wiley.com/terms-and-conditions) on Wiley Online Library for rules of use; OA articles are governed by the applicable Creative Commons License

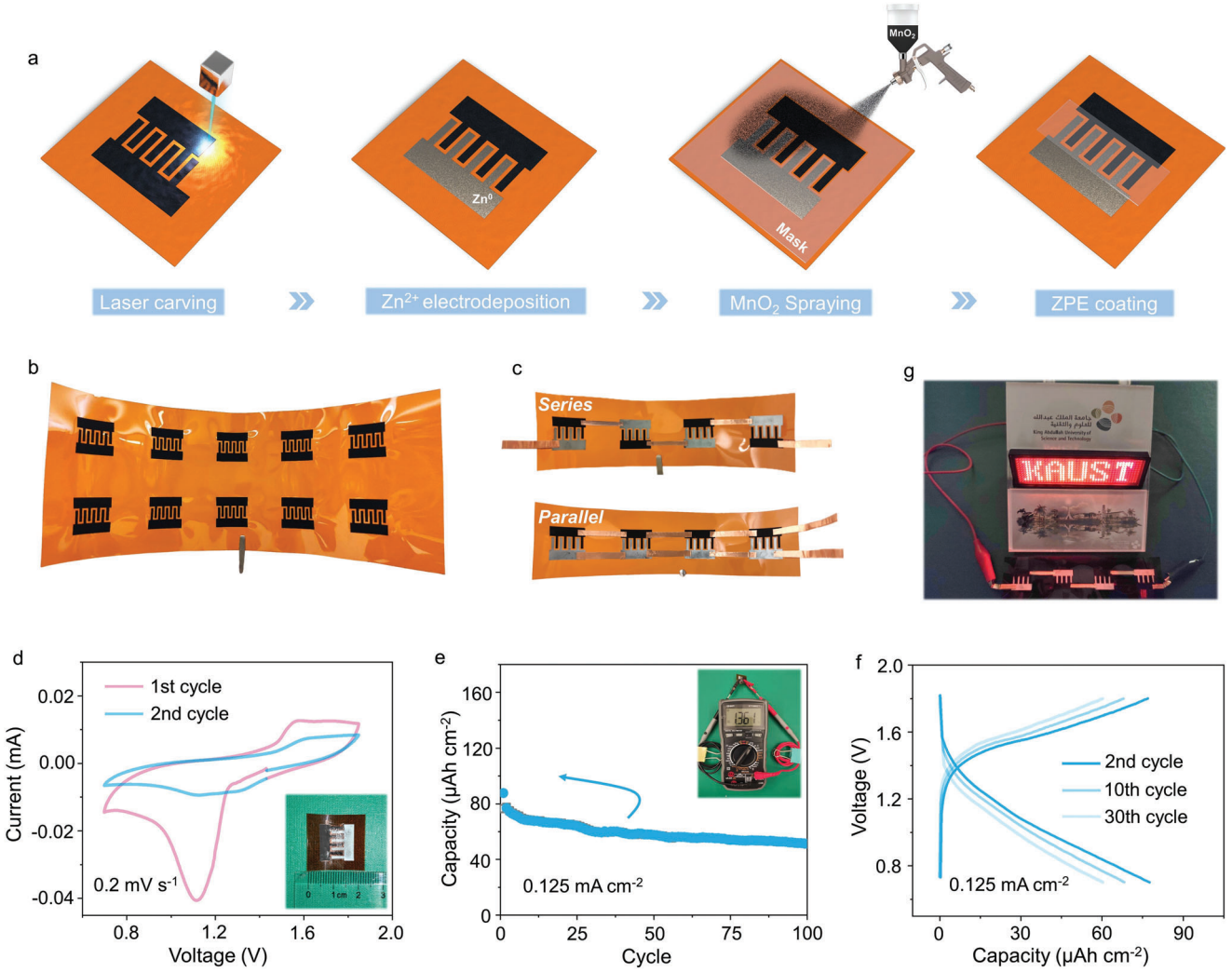

Figure 5. a) The schematics of the preparation process of the MBs. b) The integrated substrates of the MBs. c) Integrated MBs in series and in parallel form. d) The first two CV cycles of the Zn-MnO_2 MB. Inset: the digital photograph of the Zn-MnO_2 MB. e) Long-term cycling of the Zn-MnO_2 MB at a current density of 0.125 mA cm^{-2}. Inset: the OCV test of the Zn-MnO_2 MB. f) Charge-discharge curves of the Zn-MnO_2 MB at a current density of 0.125 mA cm^{-2} corresponding to Figure 5e. g) The integrated MBs in series can power a LED screen.

electrochemical performances, ZPE was employed to construct solid thin-film **m**icro **b**atteries (MBs). The fabrication process of the Zn-MnO_2 MB is depicted in **Figure 5**a. First, the 3D porous laser-induced graphene (LIG, polyimide substrate) with crossed finger patterns was carved using a CO_2 laser, which features a high electronic conductivity as that of commercial conduction carbon.[25] Then, active Zn was electrodeposited on unilateral electrodes from a typical 1 M $ZnSO_4$ aqueous solution. Next, the as-prepared MnO_2 ink was sprayed onto the opposite electrodes aided by a polytetrafluoroethylene (PTFE) mask pinpointing at the aimed area. After natural drying, ZPE was coated on the surfaces of the finger electrodes. An independent Zn-MnO_2 MB unit was thus ultimately obtained with an areal energy density of 79.2 μWh cm^{-2} (inset of Figure 5d, Figure S14, Supporting Information). XRD and SEM results prove the integrity of the sprayed MnO_2 cathode and deposited Zn anode (Figures S15–S16, Supporting Information). The facile preparation processes are of great promise for large-scale integration (Figure 5b). Multiple MBs could readily be integrated into series to increase the output voltage or into parallel to enlarge the output current, proving the desirable versatility (Figure 5c). For example, relative to a single MB with an opening circuit voltage (OCV) of 1.36 V (inset of Figure 5e), four MBs in series can access a high OCV of 5.54 V (Figure S17, Supporting Information). As anticipated, the MB displays its typical and distinct redox couples in cyclic voltammetry (CV) curves (Figure 5d). Additionally, an assessment of the cycling performance attested to the durability (Figure 5e,f). The robust interfacial coherence enabled by the high viscoelasticity was also ascertained by electrochemical impedance spectroscopy (EIS). As suggested in Figure S18, Supporting Information, the interfacial resistance encounters slight change after frequent bending. As a proof of applicability, we demonstrate that four MBs in series can drive the LED screen sustainably (Figure 5g). It should be noted that these MBs can work without capsulation given the solidity and water-retention characteristics of ZPE, highlighting the simplification of packaging procedures.

© 2023 Wiley-VCH GmbH

16146840, 2023, 21, Downloaded from https://advanced.onlinelibrary.wiley.com/doi/10.1002/aenm.202300063 by - Jilin University , Wiley Online Library on [27/03/2025]. See the Terms and Conditions (https://onlinelibrary.wiley.com/terms-and-conditions) on Wiley Online Library for rules of use; OA articles are governed by the applicable Creative Commons License

Altogether, these results provide possible guiding principles for the design of solid electrolytes for multivalent-ion batteries.

3. Conclusion

In summary, by utilizing the self-assembly ability of amphiphilic AOT anion, a plastic-crystal Zn^{2+} electrolyte with a layered architecture was developed. Comprehensive characterizations are coupled with computational simulations and electrochemistry, allowing a detailed disclosure of ion conduction nanochannels residing in interlayers. The merged water molecules play key roles in this framework, which not only position AOT anions regularly through the ion-dipole interaction, but also facilitate Zn^{2+} conduction relying on heteroleptic coordination. The constraint of AOT by long-range van der Waals forces offers a high Zn^{2+} transference number (0.73). As a result, the plastic-crystal electrolyte shows robust stretchability and desirable viscosity, promising compatible interfaces in solid batteries. The good electrochemical performances of diverse types of batteries, including Zn-Cu, Zn-Zn, and Zn-MnO_2 configurations, demonstrate the superiority of our electrolyte. A detailed comparison with the reported work demonstrates the advantage of our electrolyte (Table S4, Supporting Information). These results offer a new approach for constructing fast multivalent-ion transport channels in solid phases, taking a step towards their use in microelectronic devices.

Supporting Information

Supporting Information is available from the Wiley Online Library or from the author.

Acknowledgements

Z.Z., B.N., and Y.L. contributed equally to this work. Research reported in this publication was supported by King Abdullah University of Science and Technology (KAUST).

Conflict of Interest

The authors declare no conflict of interest.

Data Availability Statement

The data that support the findings of this study are available from the corresponding author upon reasonable request.

Keywords

ion-transport channels, layered structures, plastic-crystal electrolytes, solid batteries

Received: January 6, 2023
Revised: March 11, 2023
Published online: April 20, 2023

[1] a) M. Song, H. Tan, D. Chao, H. J. Fan, *Adv. Funct. Mater.* **2018**, *28*, 1802564; b) Z. Zhao, J. Yin, J. Yin, X. Guo, Y. Lei, Z. Tian, Y. Zhu, O. F. Mohammed, H. N. Alshareef, *Energy Storage Mater.* **2023**, *55*, 479; c) M. Qiu, P. Sun, Y. Wang, L. Ma, C. Zhi, W. Mai, *Angew. Chem., Int. Ed.* **2022**, *61*, e202210979.

[2] a) L. Ma, M. A. Schroeder, O. Borodin, T. P. Pollard, M. S. Ding, C. Wang, K. Xu, *Nat. Energy* **2020**, *5*, 743; b) Z. Zhao, J. Lai, D. T. Ho, Y. Lei, J. Yin, L. Chen, U. Schwingenschlögl, H. N. Alshareef, *ACS Energy Lett.* **2022**, *8*, 608; c) D. Lin, Y. Li, *Adv. Mater.* **2022**, *34*, 2108856.

[3] a) Z. Zhao, J. Zhao, Z. Hu, J. Li, J. Li, Y. Zhang, C. Wang, G. Cui, *Energy Environ. Sci.* **2019**, *12*, 1938; b) G. Liang, C. Zhi, *Nat. Nanotechnol.* **2021**, *16*, 854.

[4] a) L. Zhang, G. Yu, *Angew. Chem., Int. Ed.* **2021**, *60*, 15028; b) J. F. Parker, C. N. Chervin, I. R. Pala, M. Machler, M. F. Burz, J. W. Long, D. R. Rolison, *Science* **2017**, *356*, 415; c) H. Qiu, X. Du, J. Zhao, Y. Wang, J. Ju, Z. Chen, Z. Hu, D. Yan, X. Zhou, G. Cui, *Nat. Commun.* **2019**, *10*, 5374.

[5] Z. Zhao, J. Wang, Z. Lv, Q. Wang, Y. Zhang, G. Lu, J. Zhao, G. Cui, *Chem. Eng. J.* **2021**, *417*, 128096.

[6] a) G. Lu, H. Qiu, X. Du, K. K. Sonigara, J. Wang, Y. Zhang, Z. Chen, L. Chen, Y. Ren, Z. Zhao, *Chem. Mater.* **2022**, *34*, 8975; b) W. Yang, Y. Yang, H. Yang, H. Zhou, *ACS Energy Lett.* **2022**, *7*, 2515.

[7] a) L. Ma, S. Chen, N. Li, Z. Liu, Z. Tang, J. A. Zapien, S. Chen, J. Fan, C. Zhi, *Adv. Mater.* **2020**, *32*, 1908121; b) J. Yan, M. Ye, Y. Zhang, Y. Tang, C. C. Li, *Chem. Eng. J.* **2022**, *432*, 134227; c) Y. Liang, H. Dong, D. Aurbach, Y. Yao, *Nat. Energy* **2020**, *5*, 646.

[8] J. Maier, O. Wissenschaftsverlag, *Z. Phys. Chem.* **2003**, *217*, 415.

[9] a) J. Maier, *J. Phys. Chem. Solids* **1985**, *46*, 309; b) C. Liang, *J. Electrochem. Soc.* **1973**, *120*, 1289; c) J. S. Lee, S. Adams, J. Maier, *J. Electrochem. Soc.* **2000**, *147*, 2407; d) J. Maier, B. Reichert, *Ber. Bunsengesellschaft für physikalische Chem.* **1986**, *90*, 666.

[10] a) X. Zhang, H. Liu, L. Jiang, *Adv. Mater.* **2019**, *31*, 1804508; b) L. Wen, X. Zhang, Y. Tian, L. Jiang, *Sci. China: Mater.* **2018**, *61*, 1027; c) Y. Hao, X. Zhang, L. Jiang, *Nanoscale Horiz.*. **2019**, *4*, 1029.

[11] M. S. Sansom, I. H. Shrivastava, J. N. Bright, J. Tate, C. E. Capener, P. C. Biggin, *Biochim. Biophys. Acta Biomembr.* **2002**, *1565*, 294.

[12] S. Ikeda, Y. Kanbayashi, K. Nomura, A. Kasai, K. Ito, *Solid State Ionics* **1990**, *40*, 79.

[13] a) J. P. Cason, M. E. Miller, J. B. Thompson, C. B. Roberts, *J. Phys. Chem. B* **2001**, *105*, 2297; b) P. Calandra, A. Longo, V. T. Liveri, *J. Phys. Chem. B* **2003**, *107*, 25; c) F. M. Pavel, R. A. Mackay, *Langmuir* **2000**, *16*, 8568.

[14] a) P. L. Luisi, B. Straub, *Reverse Micelles: Biological and Technological Relevance of Amphiphilic Structures in Apolar Media*, Springer, New York, NY **1984**; b) K. Bhattacharyya, B. Bagchi, *J. Phys. Chem. A* **2000**, *104*, 10603.

[15] M. Pileni, *J. Phys. Chem.* **1993**, *97*, 6961.

[16] a) B. Dobraszczyk, M. Morgenstern, *J. Cereal Sci.* **2003**, *38*, 229; b) F. A. Morrison, *Understanding Rheology*, Oxford University Press, New York **2001**.

[17] a) A. Y. Malkin, A. I. Isayev, *Rheology: Concepts, Methods, and Applications*, Elsevier, Scarborough **2022**; b) T. A. Osswald, N. Rudolph, *Polymer Rheology*, Hanser Publishers, Munich, Germany **2015**.

[18] a) T. G. Mason, *Rheol. Acta* **2000**, *39*, 371; b) P. Pötschke, T. Fornes, D. Paul, *Polymer* **2002**, *43*, 3247.

[19] a) Y.-H. Zhang, C. K. Chan, *J. Phys. Chem. A* **2003**, *107*, 5956; b) B. Auer, J. Skinner, *J. Chem. Phys.* **2008**, *128*, 224511; c) Y. Yamada, K. Usui, K. Sodeyama, S. Ko, Y. Tateyama, A. Yamada, *Nat. Energy* **2016**, *1*, 16129.

[20] P. D. Moran, G. A. Bowmaker, R. P. Cooney, J. R. Bartlett, J. L. Woolfrey, *J. Mater. Chem.* **1995**, *5*, 295.

[21] a) M. Drab, E. Gongadze, V. Kralj-Iglič, A. Iglič, *Entropy* **2020**, *22*, 1054; b) K. H. Sippel, F. A. Quiocho, *Protein Sci.* **2015**, *24*, 1040;. c) L.-H. Wang, Z.-D. Zhang, C.-Y. Hong, X.-H. He, W. You, Y.-Z. You, *Adv. Mater.* **2015**, *27*, 3202; d) C. Dellago, M. M. Naor, *Comput. Phys. Commun.* **2005**, *169*, 36.

© 2023 Wiley-VCH GmbH

16146840, 2023, 21, Downloaded from https://advanced.onlinelibrary.wiley.com/doi/10.1002/aenm.202300063 by - Jilin University , Wiley Online Library on [27/03/2025]. See the Terms and Conditions (https://onlinelibrary.wiley.com/terms-and-conditions) on Wiley Online Library for rules of use; OA articles are governed by the applicable Creative Commons License

[22] a) T. Bauer, M. Köhler, P. Lunkenheimer, A. Loidl, C. Angell, *J. Chem. Phys.* **2010**, *133*, 144509;. b) D. R. MacFarlane, M. Forsyth, *Adv. Mater.* **2001**, *13*, 957.

[23] a) J. Zhang, W. Li, J. Wang, X. Pu, G. Zhang, S. Wang, N. Wang, X. Li, *Angew. Chem., Int. Ed.* **2022**, e202215654; b) S.-D. Han, S. Kim, D. Li, V. Petkov, H. D. Yoo, P. J. Phillips, H. Wang, J. J. Kim, K. L. More, B. Key, *Chem. Mater.* **2017**, *29*, 4874.

[24] a) N. Becknell, P. P. Lopes, T. Hatsukade, X. Zhou, Y. Liu, B. Fisher, D. Y. Chung, M. G. Kanatzidis, N. M. Markovic, S. Tepavcevic, *Adv. Funct. Mater.* **2021**, *31*, 2102135; b) D. Wang, L. Wang, G. Liang, H. Li, Z. Liu, Z. Tang, J. Liang, C. Zhi, *ACS Nano* **2019**, *13*, 10643; c) C. Qiu, J. Liu, H. Liu, X. Zhu, L. Xue, S. Li, M. Ni, Y. Zhao, T. Wang, S. V. Savilov, *Small Methods* **2022**, 2201142; d) C. Qiu, X. Zhu, L. Xue, M. Ni, Y. Zhao, B. Liu, H. Xia, *Electrochim. Acta* **2020**, *351*, 136445.

[25] a) Y. Lei, W. Zhao, Y. Zhu, U. Buttner, X. Dong, H. N. Alshareef, *ACS Nano* **2022**, *16*, 1974; b) N. J. Dudney, *Electrochem. Soc. Interface* **2008**, *17*, 44.

© 2023 Wiley-VCH GmbH

16146840, 2023, 21, Downloaded from https://advanced.onlinelibrary.wiley.com/doi/10.1002/aenm.202300063 by - Jilin University , Wiley Online Library on [27/03/2025]. See the Terms and Conditions (https://onlinelibrary.wiley.com/terms-and-conditions) on Wiley Online Library for rules of use; OA articles are governed by the applicable Creative Commons License